

**Coral thermal microclimate:
Investigating the effects of irradiance, flow and
coral thermophysical properties**

Isabel Margarita Jimenez-Denness

(Dipl. Eng. Physics)

A thesis submitted for the degree of Doctor of Philosophy

Department of Environmental Sciences
University of Technology, Sydney, Australia

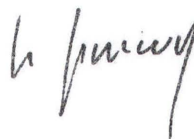
January 2009

Certificate

I certify that this thesis has not already been submitted for any degree and is not being submitted as part of candidature for any other degree.

I also certify that the thesis has been written by me. Any help that I have received in my research work and the preparation of the thesis itself has been acknowledged. All information sources and literature used are indicated in the thesis.

Signature of Candidate

A handwritten signature in black ink, appearing to read 'I. M. Jimenez-Denness', written in a cursive style.

I. M. Jimenez-Denness

Acknowledgements

I first would like to thank my principal supervisor, Assoc. Prof. Peter Ralph for continuous support, indispensable advice and remarkable patience throughout my PhD. I also want to thank Prof. Tony Larkum for his encouragement and precious advice, and Prof. Michael Kühl for teaching me microsensor techniques and for contributing to make my first field campaign a very inspiring one. Prof. Greg Skilbeck provided indispensable assistance in the materials testing component of my project, and all my supervisors contributed inspiring and stimulating discussions throughout this journey.

I am very grateful for the advice and assistance of Rod Hungerford and Norman Booth in the preparation of samples and the measurement of skeleton thermal diffusivity. The help of Greg Evans, Paul Fanos and Greg Dalsanto in the maintenance and preparation of equipment was instrumental in the timely completion of field work. I also want to extend my gratitude to the staff at Heron Island Research Station for their generous assistance during field campaigns, and to Neil Ralph for constructing many components of laboratory and field equipment. I especially want to thank members of the Aquatic Photosynthesis Group for the many good laughs these past few years, and occasionally helping me keep my sanity during field campaigns.

The opportunity to embark on this project was first made possible by an International Postgraduate Research Scholarship and a Faculty of Science Stipend, awarded to me by the University of Technology, Sydney. I was able to attend conferences thanks to financial support from the Australian Coral Reef Society and internal research allowances from the University of Technology, Sydney.

Finally, I want to thank my family and friends, here and abroad, for support, encouragement and the occasional healthy dose of gossip. To Simon, thank you for your unwavering, generous and uplifting encouragements, for putting up with the stress, frustrations and financial hardship of this journey, and especially for making me laugh through panic attacks. To my mum, thank you for understanding and accepting my relocation to the other side of the world, I know it wasn't easy, and thank you for the regular shipments of Swiss chocolate, that got me through the toughest spells of writer's block.

Contents

Certificate	i
Acknowledgements	ii
Table of contents	iii
List of figures	vii
List of tables	xiv
Abstract	xvi
1 Introduction	1
1.1 Coral reefs in an era of climatic warming	1
1.2 Microclimatic controls of coral physiology	2
1.3 Bleaching patterns and possible links to the thermal microclimate	4
1.3.1 Intraspecific bleaching patterns	4
1.3.2 Interspecific bleaching patterns	4
1.4 A biophysical approach	5
1.5 Thesis outline	6
2 Theoretical and experimental overview of the thermal environment of corals	8
2.1 Introduction	8
2.2 Theoretical considerations	10
2.2.1 Heat budget of a coral exposed to solar radiation and water flow	10
2.2.2 Diffusive and thermal boundary layers	15
2.2.3 Heat and oxygen flux across the thermal and diffusive boundary layers	16
2.3 Materials and Methods	18
2.3.1 Corals	18

2.3.2	Temperature microenvironment	18
2.3.3	Solar heating	20
2.3.4	<i>In situ</i> temperature dynamics	20
2.4	Results	22
2.4.1	Transient response	22
2.4.2	Steady state experiments	23
2.4.3	Thermal boundary layer	24
2.4.4	<i>In situ</i> temperature dynamics	28
2.5	Discussion	31
2.5.1	Boundary layers	33
2.5.2	Influence of flow rate	34
2.5.3	Size and shape of corals	35
2.5.4	Implications for mass coral bleaching	37
3	<i>In situ</i> thermal dynamics of shallow water corals	40
3.1	Introduction	40
3.2	Materials and Methods	42
3.2.1	Site and sampling periods	42
3.2.2	Coral specimens	42
3.2.3	Coral optical properties	42
3.2.4	Coral temperature measurements	43
3.2.5	Coral photosynthetic health	44
3.2.6	Statistical analysis	44
3.3	Results	45
3.3.1	Noon low tide experiments	45
3.3.2	Noon high tide experiment	49
3.3.3	Chlorophyll <i>a</i> fluorescence measurements	50
3.4	Discussion	51
3.4.1	Coral thermal dynamics	51
3.4.2	Interspecific differences	52
3.4.3	Physiological implications	53

3.5	Conclusion	54
4	Effects of flow and colony morphology on the thermal boundary layer of corals	55
4.1	Introduction	55
4.2	Materials and methods	57
4.2.1	Corals	57
4.2.2	Boundary layer measurements	58
4.2.3	Polyp-scale thermal microenvironment	58
4.2.4	Flow experiment	58
4.2.5	Dimensional analysis of heat and mass transfer	59
4.2.6	Coral reflectance spectra	60
4.2.7	Statistical analysis	61
4.3	Results	62
4.3.1	Thermal boundary layer mapping	62
4.3.2	Coral surface temperature	63
4.3.3	Surface oxygen concentration	65
4.3.4	Thermal and diffusive boundary layers	66
4.3.5	Dimensional analysis of heat and mass transfer	67
4.3.6	Coral absorptivity	68
4.4	Discussion	69
4.4.1	Flow effects on coral surface temperature	69
4.4.2	Intra-colonial heterogeneity in thermal boundary layer	70
4.4.3	Inter-specific variability in coral heat budget	71
4.4.4	Heat versus mass transfer	72
4.4.5	Dimensional analysis as a modelling tool	74
4.4.6	Extrapolation to field conditions	75
4.5	Conclusion	75
5	Thermal effects of coral optical characteristics	77
5.1	Introduction	77
5.2	Materials and Method	79

5.2.1	Corals	79
5.2.2	Temperature measurements	80
5.2.3	Bleaching experiment	80
5.2.4	Coral thermal action spectrum	82
5.2.5	Statistical analysis	83
5.3	Results	84
5.3.1	Physiological response to the bleaching treatment	84
5.3.2	Coral optical characteristics: reflectance spectra	85
5.3.3	Coral thermal exposure and heat budget	87
5.3.4	Coral thermal action spectrum	88
5.4	Discussion	91
5.4.1	Tissue light absorption	91
5.4.2	Potential influence of the skeleton	93
5.4.3	Interspecific differences in coral heat budget	93
5.4.4	Bleaching effects on coral tissue thermal exposure	95
5.4.5	Thermal effects of the spectral quality of absorbed light	95
5.5	Conclusion	98
6	A thermal model for corals	100
6.1	Introduction	100
6.2	Materials and Methods	103
6.2.1	Model development	103
6.2.2	Parameter measurements	106
6.2.3	Model validation	108
6.2.4	Sensitivity analysis	108
6.2.5	Experimental procedures	109
6.3	Results	112
6.3.1	Thermo-physical properties of corals	112
6.3.2	Model validation	113
6.3.3	Sensitivity analysis	114
6.3.4	Size and shape effects	116

6.3.5	Field applications	118
6.4	Discussion	122
6.4.1	Thermal role of the skeleton	122
6.4.2	Limitations	124
6.4.3	Field experiments	126
6.5	Conclusion	129
7	General Discussion	130
7.1	Thesis outcomes	131
7.1.1	Insights from modelling heat transfer in corals	131
7.1.2	Insights from microscale temperature measurements	132
7.1.3	Insights from absorptivity studies	133
7.1.4	Insights from field studies of <i>in situ</i> coral thermal dynamics . . .	134
7.2	Microclimatic effects on physiology and possible implications for bleaching	136
7.2.1	Intraspecific variability	136
7.2.2	Interspecific variability	137
7.3	Summary of key findings	139
7.4	Conclusion	140
	References	141
	Appendices	164
A	Measuring skeletal thermophysical properties	166
A.1	Skeleton specific heat	166
A.2	Skeleton thermal diffusivity	168

List of Figures

- 2.1 Conceptual diagrams of the relevant heat fluxes (and associated parameters) in (a) a whole coral divided into sun exposed and shaded regions (of surface areas A_1 and A_2 , respectively) and (b) in a small portion of surface tissue: radiation absorption (absorptivity, α); heat loss to the skeleton by conduction (skeleton conductance, K); heat loss to the water column by convection (convection coefficient, h). Schematic temperature profile, where T_{tissue} is the coral tissue temperature, T_{water} is the water temperature away from the boundary layer, and T_{skel} is the skeleton core temperature. Definition of the effective thickness (δ) of the thermal boundary layer (TBL), where ΔT is the coral surface warming ($T - T_{water}$) 11

- 2.2 Diagram of experimental setup used for measurements of temperature and oxygen microenvironment. The temperature microsensor was mounted on a motorized micromanipulator (MM) and connected to a thermocouple meter (see text). For the O_2 profiles, the temperature microsensor was replaced by an O_2 microelectrode connected to a picoammeter (see text). . 19

- 2.3 Polyp warming in response to a dark-light shift. (a) Hemispherical *Cyphastrea serailia* (50 mm diameter) and (b) Thin branch of *Seriatopora hystrix* (3 mm branch thickness). 22

2.4	Surface warming of branching <i>Stylophora pistillata</i> and hemispherical <i>Porites lobata</i> placed in a flow chamber (0.2 cm s^{-1}) under direct solar irradiance.	23
2.5	Temperature and oxygen boundary layers for the hemispherical coral <i>Favia</i> sp., measured in a flow chamber (0.2 cm s^{-1}) under artificial light. Temperature (0.2 cm s^{-1} ; $2080 \mu\text{mol photons m}^{-2} \text{ s}^{-1}$); oxygen (0.2 cm s^{-1} ; $480 \mu\text{mol photons m}^{-2} \text{ s}^{-1}$).	24
2.6	Effect of flow on the temperature profile for (a) a hemispherical <i>Favia</i> sp. and (b) a branch of <i>Stylophora pistillata</i> , measured in a flow chamber and artificial light (400 - 730 nm, $2080 \mu\text{mol photons m}^{-2} \text{ s}^{-1}$).	25
2.7	Effect of irradiance on the temperature profile in the thermal boundary layer above a hemispherical <i>Porites lobata</i> ($n = 4$), measured in a flow chamber (0.2 cm s^{-1}) under artificial light.	27
2.8	<i>In situ</i> temperature dynamics of <i>Cyphastrea serailia</i> and <i>Porites cylindrica</i> colonies during days of noon low tide and days of noon high tide. (a, b) Temperature gradient between coral skeleton (5 mm depth) and water. (c, d) Incident PAR at the depth of the corals for the corresponding days. The horizontal lines above the curve represent 2 h intervals centred on the time of high tide (upper series) and low tide (lower series). (e,f) Bulk water temperature.	29
3.1	<i>In situ</i> temperature measurements. (a) Submersible temperature logging equipment (photo: I. Jimenez) and (b) close-up of a <i>P. cylindrica</i> colony with inserted temperature sensor (photo: G. Holmes).	43

3.2	<i>In situ</i> temperature dynamics of hemispherical <i>Porites lobata</i> and branching <i>Porites cylindrica</i> colonies during 4-day periods of noon low Spring tide in January and November 2007. (a, b) Incident PAR measured at the depth of corals and tidal height at Heron Island. (c, d) Water temperature. (e-h) Temperature gradient between coral surface and water for the (e, f) <i>P. lobata</i> and (g, h) <i>P. cylindrica</i> specimens (Average \pm SE, n=4 and 5 in January and November, respectively).	46
3.3	Temperature dynamics of the <i>Porites lobata</i> on 22 November 2007 (Average \pm SE, n=5). Maxima in coral surface warming are indicated by arrows: (a) 14:30 h and (b) 15:30, and a sun indicates solar noon. Inset: Temperature of water (solid line) and corals (dashed line).	48
3.4	<i>In situ</i> temperature dynamics of hemispherical <i>Porites lobata</i> and branching <i>Porites cylindrica</i> colonies during a 4-day period of noon high tide in November 2007. (a) Incident PAR measured at the depth of corals and tidal height at Heron Island. (b) Water temperature. (c, d) Temperature gradient between coral surface and water for the (c) <i>P. lobata</i> and (d) <i>P. cylindrica</i> specimens (Average \pm SE, n=5).	49
3.5	Plots of (a) tidal height and underwater PAR during the noon-low and noon-high tide sampling periods (November 2007), and (b) quantum yield of PSII for <i>Porites lobata</i> and <i>Porites cylindrica</i> (averages \pm SE, n = 5). .	50
4.1	Contour maps of the thermal boundary layer over (a) two neighbouring polyps of <i>Platygyra</i> sp. and (b) an individual polyp of <i>Favia</i> sp., under flow and light conditions of 1 cm s^{-1} and 430 W m^{-2} ($1500 \mu\text{mol photons m}^{-2} \text{ s}^{-1}$), respectively. For better illustration, the map for <i>Favia</i> sp. was duplicated by right symmetry. (c) Schematic diagram of polyps of the <i>Platygyra</i> sp. and <i>Favia</i> sp. specimens.	62

- 4.2 Effect of flow on the tissue surface warming of *Stylophora pistillata* branches (n = 9) and hemispherical colonies of *Porites lobata* (n = 10), measured in a flow chamber under high irradiance (1500 W m^{-2} ; $2500 \mu\text{mol photons m}^{-2} \text{ s}^{-1}$). Averages \pm SE are shown. The least square power-law regressions are: $\Delta T = 0.11 v^{-0.47}$, $r^2 = 0.99$ and $\Delta T = 0.31 v^{-0.59}$, $r^2 = 0.98$ for *S. pistillata* and *P. lobata*, respectively. 63
- 4.3 Coral surface warming of *Stylophora pistillata* branches (n = 9) and hemispherical colonies of *Porites lobata* (n = 10) plotted against the thickness of the thermal boundary layer, measured under 1500 W m^{-2} ($2500 \mu\text{mol photons m}^{-2} \text{ s}^{-1}$) irradiance and flows ranging between $0.3 - 5.0 \text{ cm s}^{-1}$. The least square regression lines are: $\Delta T = 1.1 \cdot 10^{-4} \delta_{TBL} - 6.9 \cdot 10^{-2}$, $r^2 = 0.73$, and $\Delta T = 3.0 \cdot 10^{-4} \delta_{TBL} - 2.5 \cdot 10^{-2}$, $r^2 = 0.73$ for *S. pistillata* and *P. lobata*, respectively. 64
- 4.4 Effect of flow on the surface O_2 concentration of *Stylophora pistillata* branches (n = 7) and hemispherical colonies of *Porites lobata* (n = 8), measured in a flow chamber and exposed to $430 \mu\text{mol photons m}^{-2} \text{ s}^{-1}$. Averages \pm SE are shown. The least square power-law regressions are: $C_s = 161 v^{-0.20}$, $r^2 = 0.95$ and $C_s = 180 v^{-0.18}$, $r^2 = 0.99$ for *S. pistillata* and *P. lobata*, respectively. 65
- 4.5 Effect of flow on δ_{TBL} and δ_{DBL} over *Stylophora pistillata* branches (n = 9) and hemispherical colonies of *Porites lobata* (n = 10). Averages \pm SE are shown. The least square power-law regressions are: a) *S. pistillata*: $TBL = 1183 v^{-0.31}$, $r^2 = 0.95$ and $DBL = 463 v^{-0.73}$, $r^2 = 0.88$; b) *P. lobata*: $TBL = 1294 v^{-0.41}$, $r^2 = 0.99$ and $DBL = 297 v^{-0.72}$, $r^2 = 0.97$ 66

4.6	Non-dimensional representation of Fig. 4.5, i.e. dimensional analysis of flow-assisted transfer of a) heat and b) mass for colonies of <i>Porites lobata</i> ($n = 10 \pm \text{SE}$) and <i>Stylophora pistillata</i> ($n = 9 \pm \text{SE}$). <i>Nu</i> : Nusselt number; <i>Sh</i> : Sherwood number; <i>Re</i> : Reynolds number. The slopes of the plots were a) <i>Nu-Re</i> : 0.31 and 0.41 and b) <i>Sh-Re</i> : 0.73 and 0.72 for <i>S. pistillata</i> and <i>P. lobata</i> , respectively. (See text, 4.2.5, for the calculation of the dimensionless parameters as a function of coral dimensions, flow velocity, and boundary layer thicknesses.)	67
5.1	Relative change in photochemical efficiency (F_v/F_m) in relation to pre-treatment responses ($n=3 \pm \text{SE}$) of the control (dashed lines) and treatment (solid lines) of <i>S. pistillata</i> (triangles) and <i>P. lobata</i> (circles). The three days of temperature ramping are indicated as the light grey bar, and the control (25 °C) and treatment (32 °C) as the dark grey bar.	84
5.2	Spectral reflectance of a, c) <i>P. lobata</i> and b,d) <i>S. pistillata</i> measured during the bleaching treatment. Data were normalized to a, b) the radiance from a reference white diffusing surface and subsequently to c,d) the reflectance at 750 nm. Averages $\pm \text{SE}$ are shown ($n = 3$).	86
5.3	Action spectra of coral surface warming for bleached and control specimens of (a,b,c) <i>S. pistillata</i> and (d,e,f) <i>P. lobata</i> . Coral surface warming at each wavelength was normalized to (a,d) an equivalent quantum irradiance of $1500 \mu\text{mol photons m}^{-2} \text{s}^{-1}$ and (b,e) to an equivalent irradiance of 1000 W m^{-2} . Difference in spectral absorptivity between the bleached and healthy coral samples are shown (c,f).	89

5.4	a) Spectral reflectance and b) thermal action spectrum of the grey and yellow morphs of <i>P. cylindrica</i> . Spectral reflectance was normalized to the reflectance at 750 nm. The measured coral surface warming at each wavelength was normalized to a quantum irradiance of 1500 $\mu\text{mol photons m}^{-2} \text{s}^{-1}$	90
6.1	Geometrical models used for the simulation of heat transfer in branching and hemispherical coral morphologies.	103
6.2	Model mesh structure showing the butterfly topology in the cross section of a cylindrical branch (left, node number: 29700), and a coarse version of the meshed hemisphere (right, node number: 67000).	106
6.3	Measured and predicted surface warming (ΔT) of (a) hemispherical and (b) cylindrical corals. The dashed line indicates a 1:1 relationship.	113
6.4	Surface warming ($^{\circ}\text{C}$) as a function of flow velocity and irradiance for hemispheres (a, b, c) and cylinders (d, e, f) of various diameters.	116
6.5	Time constant of coral surface warming as a function of coral diameter at flow velocities of 0.2 and 5 cm s^{-1}	117
6.6	Partitioning of heat loss from the tissue layer by convection to the surrounding water (Q_{conv}) and conduction into the skeleton (Q_{cond}) for a) a thin cylinder (0.5 cm diameter) and b) a hemisphere (10 cm diameter).	118
6.7	Effect of depth on the surface warming of hemispheres 1 and 10 cm in diameter; for two optical types of water: (a,b) $k_d = 0.05$ and (c,d) 0.5 m^{-1} ; and two flow velocities: (a,c) 0.2 and (b,d) 5 cm s^{-1}	119

6.8	Predicted surface warming of a hemispherical (10 cm diameter; solid dark line) and cylindrical coral (1 cm diameter; solid green line), using computed water level and irradiance, together with flow velocity estimates (see section 6.2.5). Measured values of <i>in situ</i> surface warming of colonies of <i>P. lobata</i> and <i>P. cylindrica</i> (n=4) are shown for comparison. Experimental data were collected in the shallow reef flat (depth <3 m) at Heron Island in the Southern Great Barrier Reef, as described in Chapter 2.	120
6.9	Contour plots of the computed (a,b) maximum surface warming (°C) and (c,d) cumulated heat exposure (degree-heating-hour) on the horizontal projection of a hemispherical coral (20 cm diameter). Low tide at noon (a,c) and in the morning (b,d).	121
A.1	Diagram of the experimental set up for the determination of the thermal diffusivity of coral skeletons.	169

List of Tables

- 1 List of terms. xix

- 2.1 Constants of the model. 14

- 2.2 Effect of flow on coral surface warming (ΔT), boundary layer thick-
 ness (δ), convective heat flux (Q), and convection coefficient (h) of the
 hemispherical corals *Favia* sp. and *Porites lobata* and the branching *Sty-*
 lophora pistillata. Mean \pm standard error (SE) ($n=3$). 26

- 2.3 Effect of irradiance on coral surface warming (ΔT), boundary layer thick-
 ness (δ), convective heat flux (Q), and convection coefficient (h) of a
 Porites lobata colony. Mean \pm standard error (SE) ($n=4$). 28

- 5.1 Zooxanthellae density (cells $\text{cm}^{-2} \times 10^6$), absorptivity (non dimensional)
 and coral surface warming ($^{\circ}\text{C}$) in *P. lobata* and *S. pistillata*. Measure-
 ments were taken from the end of the control treatment (control), the first
 measurement prior to exposure to bleaching conditions (pretreatment) and
 the end of the exposure period (treatment). Averages \pm SE shown ($n = 3$),
 and significant differences ($p < 0.05$) are denoted with superscript values. 85

5.2	Absorbed irradiance (Q_{rad}) and heat loss by convection (Q_{conv}) in <i>P. lobata</i> and <i>S. pistillata</i> exposed to an irradiance of $1800 \mu\text{mol photons m}^{-2} \text{s}^{-1}$ (450 W m^{-2}) and a flow velocity of 0.75 cm s^{-1} . Measurements were taken at the end of the control treatment (control) and the exposure period (exposure). Q_{rad} was estimated as ($\alpha \times 450 \text{ W m}^{-2}$), and Q_{conv} was estimated as described in Chapter 2. Numbers represent averages \pm SE ($n = 3$).	88
6.1	Thermo-physical properties of coral skeletons of <i>Stylophora pistillata</i> , <i>Porites lobata</i> and <i>Porites cylindrica</i> : thermal diffusivity (κ , $10^{-7} \text{ m}^{-2} \text{s}^{-1}$), specific heat (c , $\text{J kg}^{-1} \text{K}^{-1}$), density (ρ , kg m^{-3}) and thermal conductivity (k , $\text{W m}^{-1} \text{K}^{-1}$). Averages \pm SE are shown ($n = 5$), and significant differences ($p < 0.05$, ANOVA) are denoted with superscript letters. .	112
6.2	Model sensitivity analysis for steady-state surface warming (ΔT) of two hemispherical colonies 20 and 100 cm in diameter, at low and high flow velocities (0.2 and 5 cm s^{-1} , respectively). Change in ΔT ($^{\circ}\text{C}$) of colony apex for a $\pm 10\%$ change in each parameter.	114
6.3	Model sensitivity analysis for the transient response time (τ) of a large hemispherical colony (100 cm diameter) at low and high flow velocities (0.2 and 5 cm s^{-1} , respectively). Change in τ (s) of colony apex for a $\pm 10\%$ change in each parameter.	115

Abstract

Understanding the processes that drive the variability in thermal tolerance among scleractinian corals is key to predicting the impacts of rising worldwide temperatures on coral reefs. This thesis explores the thermal microclimate of corals, and specifically examines the thermal effects of environmental conditions of flow and irradiance, combined with the optical, thermal and morphological characteristics of individual coral colonies.

The temperature of branching (*Porites cylindrica*) and hemispherical (*Porites lobata* and *Cyphastrea serailia*) coral species was monitored on a shallow reef flat in the Southern Great Barrier Reef. This revealed a strong diurnal and tidal pattern in solar heating of corals, whereby maximum coral surface warming of $\sim +0.6$ °C occurred during low Spring tides, under conditions of high irradiance and low water flow.

Microsensor temperature measurements were used to demonstrate for the first time that at flow velocities $< 5 \text{ cm s}^{-1}$ heat transfer at the surface of corals was controlled by a thermal boundary layer (TBL). Dimensionless analysis of heat transfer (Nusselt-Reynolds number plots) confirmed that convective heat transfer at the surface of hemispherical *Porites lobata* and branching colonies (*Stylophora pistillata*) occurred through a laminar boundary layer, consistent with predictions from engineering theory for simple geometrical objects. For topographically more complex corals (*Favia* and *Platygyra* sp.) both the TBL thickness and the surface temperature was spatially heterogeneous.

Temperature and spectral reflectance measurements were used to investigate close links between the thermal and optical properties of corals. Coral surface temperature could be expressed as a linear function of the tissue's absorptivity, but this relationship was species-specific, and highlighted the thermal importance of the skeleton. The spectral composition of light was important in determining the magnitude of coral surface warming, and short wavelengths ($< 500 \text{ nm}$) had the greatest heating efficiency.

Finally, a mechanistic thermal model of corals identified both irradiance absorption and convective heat loss as the major controlling parameters of coral surface warming. Conductive heat transfer into the skeleton was a negligible portion of the overall heat budget, except for small coral diameters ($\sim 1 \text{ cm}$). Experimental and theoretical results throughout this thesis revealed that the surface warming of hemispherical coral species

was greater than that of branching species, and indicates that massive species may tolerate temperatures greater than previously thought. In light of the greater bleaching resistance of massive compared to branching species, this warrants further investigation into the effects of small temperature differences on the physiological response of morphologically distinct, bleaching sensitive and resistant coral species.

Table 1: List of terms.

α	Tissue absorptivity
δ	Boundary layer thickness (μm or mm)
ϵ	Surface emissivity
ρ	Density ($kg\ m^{-3}$)
σ	Stefan-Boltzmann constant ($5.673 \times 10^{-8}\ Wm^{-2}K^{-1}$)
τ	Transient response time (s)
ΔT	Warming: $T - T_{water}$ (K or C)
$\Delta T_{m\ tissue}$	Maximum surface warming (K or C)
$\Delta T_{m\ skel}$	Maximum skeleton warming (K or C)
$\Delta F/F_m'$	Effective quantum yield of PSII
κ	Skeleton thermal diffusivity (m^2s^{-1})
ν	Water kinematic viscosity (m^2s^{-1})
ANOVA	Analysis of Variance
A_1	Surface area of sun-exposed tissue (m^2)
A_2	Surface area of shaded tissue (m^2)
A	Total coral surface area (m^2)
Bi	Biot number
c	Skeleton specific heat capacity ($Jkg^{-1}K^{-1}$)
DBL	Diffusive boundary layer
E	Incident irradiance (Wm^{-2})
F	Variable chlorophyll <i>a</i> fluorescence
F_m'	Maximum fluorescence in light
F_v/F_m	Dark adapted maximum quantum yield of PSII
h	Convection coefficient ($Wm^{-2}K^{-1}$)
k	Conductivity ($Wm^{-2}K^{-1}$)
K	Skeleton conductance ($Wm^{-2}K^{-1}$)
Le	Lewis number
Nu	Nusselt number
PAR	Photosynthetically active radiation
PSII	Photosystem II
q_{rad}	Absorbed radiation flux (Wm^{-2})
q_{cond}	Conduction flux from the tissue to the skeleton (Wm^{-2})
$q_{conv\ 1}$	Convection flux from the tissue to the water (Wm^{-2})
$q_{conv\ 2}$	Convection flux from the skeleton to the water (Wm^{-2})
Re	Reynolds number
Sh	Sherwood number
TBL	Thermal boundary layer
T_{tissue}	Tissue temperature (K)
T_{skel}	Skeleton temperature (K)
T_{water}	Water temperature (K)